Femtosecond thin disk laser oscillator with pulse energy beyond the 10-microjoule level

S. V. Marchese, [*] **C. R. E. Baer, A. G. Engqvist, S. Hashimoto, D. J. H. C. Maas, M. Golling, T. Südmeyer, and U. Keller**

Department of Physics, Institute of Quantum Electronics, ETH Zurich, 8093 Zurich, Switzerland
[*]Corresponding author: marchese@phys.ethz.ch

Abstract: We report on a passively mode-locked Yb:YAG thin disk laser oscillator that generates 11.3-µJ pulses without the use of any additional external amplification. A repetition rate of 4 MHz is obtained using a 23.4-m-long multiple-pass cavity that extends the resonator length to a total of 37 m. The nearly transform-limited pulses at 45 W of average output power have a duration of 791 fs with a 1.56-nm-broad spectrum centered at 1030 nm. The laser is operated in a helium atmosphere to eliminate the air nonlinearity inside the resonator that previously limited the pulse energy.

©2008 Optical Society of America

OCIS codes: (140.3480) Lasers, diode-pumped; (140.3580) Lasers, solid-state; (140.4050) Mode-locked lasers

---

References and links

1. B. N. Chichkov, C. Momma, S. Nolte, F. von Alvensleben, and A. Tünnermann, "Femtosecond, picosecond and nanosecond laser ablation of solids," Appl. Phys. A **63**, 109-115 (1996).
2. S. V. Marchese, S. Hashimoto, C. R. E. Baer, M. S. Ruosch, R. Grange, M. Golling, T. Südmeyer, U. Keller, G. Lépine, G. Gingras, and B. Witzel, "Passively mode-locked thin disk lasers reach 10 microjoules pulse energy at megahertz repetition rate and drive high field physics experiments," presented at the Conference on Lasers and Electro-Optics (Europe), Munich, Germany, talk CF3-2-MON, 2007.
3. A. Giesen, H. Hügel, A. Voss, K. Wittig, U. Brauch, and H. Opower, "Scalable Concept for Diode-Pumped High-Power Solid-State Lasers," Appl. Phys. B **58**, 365-372 (1994).
4. U. Keller, D. A. B. Miller, G. D. Boyd, T. H. Chiu, J. F. Ferguson, and M. T. Asom, "Solid-state low-loss intracavity saturable absorber for Nd:YLF lasers: an antiresonant semiconductor Fabry-Perot saturable absorber," Opt. Lett. **17**, 505-507 (1992).
5. U. Keller, K. J. Weingarten, F. X. Kärtner, D. Kopf, B. Braun, I. D. Jung, R. Fluck, C. Hönninger, N. Matuschek, and J. Aus der Au, "Semiconductor saturable absorber mirrors (SESAMs) for femtosecond to nanosecond pulse generation in solid-state lasers," IEEE J. Sel. Top. Quantum Electron. **2**, 435-453 (1996).
6. E. Innerhofer, T. Südmeyer, F. Brunner, R. Häring, A. Aschwanden, R. Paschotta, U. Keller, C. Hönninger, and M. Kumkar, "60 W average power in 810-fs pulses from a thin-disk Yb:YAG laser," Opt. Lett. **28**, 367-369 (2003).
7. F. Brunner, E. Innerhofer, S. V. Marchese, T. Südmeyer, R. Paschotta, T. Usami, H. Ito, S. Kurimura, K. Kitamura, G. Arisholm, and U. Keller, "Powerful red-green-blue laser source pumped with a mode-locked thin disk laser," Opt. Lett. **29**, 1921-1923 (2004).
8. E. Innerhofer, F. Brunner, S. V. Marchese, R. Paschotta, G. Arisholm, S. Kurimura, K. Kitamura, T. Usami, H. Ito, and U. Keller, "Analysis of nonlinear wavelength conversion system for a red-green-blue laser-projection source," J. Opt. Soc. Am. B **23**, 265-275 (2006).
9. A. Killi, A. Steinmann, J. Dörring, U. Morgner, M. J. Lederer, D. Kopf, and C. Fallnich, "High-peak-power pulses from a cavity-dumped Yb:KY(WO$_4$)$_2$ oscillator," Opt. Lett. **30**, 1891-1893 (2005).
10. G. Palmer, M. Siegel, A. Steinmann, and U. Morgner, "Microjoule pulses from a passively mode-locked Yb:KY(WO$_4$)$_2$ thin-disk oscillator with cavity dumping," Opt. Lett. **32**, 1593-1595 (2007).
11. F. Röser, J. Rothhard, B. Ortac, A. Liem, O. Schmidt, T. Schreiber, J. Limpert, and A. Tünnermann, "131 W 220 fs fiber laser system," Opt. Lett. **30**, 2754-2756 (2005).
12. L. Shah, M. E. Fermann, J. W. Dawson, and C. P. J. Barty, "Micromachining with a 50 W, 50 µJ, sub-picosecond fiber laser system," Opt. Express **14**, 12546-12551 (2006).
13. S. V. Marchese, T. Südmeyer, M. Golling, R. Grange, and U. Keller, "Pulse energy scaling to 5 µJ from a femtosecond thin disk laser," Opt. Lett. **31**, 2728-2730 (2006).
14. D. Herriott, H. Kogelnik, and R. Kompfner, "Off-Axis Paths in Spherical Mirror Interferometers," Appl. Opt. **3**, 523-526 (1964).

15. A. Giesen and J. Speiser, "Fifteen Years of Work on Thin-Disk Lasers: Results and Scaling Laws," IEEE J. Sel. Top. Quantum Electron. **13**, 598-609 (2007).
16. A. Tünnermann, H. Zellmer, W. Schöne, A. Giesen, and K. Contag, "New Concepts for Diode-Pumped Solid-State Lasers," in *Vol. 78 of Topics in Applied Physics*, R. Diehl, ed. (Springer-Verlag, 2000), p. 369-408.
17. F. X. Kärtner, I. D. Jung, and U. Keller, "Soliton Mode-Locking with Saturable Absorbers," IEEE J. Sel. Top. Quantum Electron. **2**, 540-556 (1996).
18. E. T. J. Nibbering, G. Grillon, M. A. Franco, B. S. Prade, and A. Mysyrowicz, "Determination of the inertial contribution to the nonlinear refractive index of air, N_2, and O_2 by use of unfocused high-intensity femtosecond laser pulses," J. Opt. Soc. Am. B **14**, 650-660 (1997).
19. R. Adair, L. L. Chase, and S. A. Payne, "Nonlinear refractive index of optical crystals," Phys. Rev. B **39**, 3337-3350 (1989).
20. V. Magni, "Multielement stable resonators containing a variable lens," J. Opt. Soc. Am. A **4**, 1962-1969 (1987).
21. S. H. Cho, B. E. Bouma, E. P. Ippen, and J. G. Fujimoto, "Low-repetition-rate high-peak-power Kerr-lens mode-locked Ti:Al_2O_3 laser with a multiple-pass cavity," Opt. Lett. **24**, 417-419 (1999).
22. S. Naumov, A. Fernandez, R. Graf, P. Dombi, F. Krausz, and A. Apolonski, "Approaching the microjoule frontier with femtosecond laser oscillators," New J. Phys. **7**, 216 (2005).
23. S. Dewald, T. Lang, C. D. Schroter, R. Moshammer, J. Ullrich, M. Siegel, and U. Morgner, "Ionization of noble gases with pulses directly from a laser oscillator," Opt. Lett. **31**, 2072-2074 (2006).
24. A. M. Kowalevicz, A. Sennaroglu, A. T. Zare, and J. G. Fujimoto, "Design principles of *q*-preserving multipass-cavity femtosecond lasers," J. Opt. Soc. Am. B **23**, 760-770 (2006).
25. C. Hönninger, R. Paschotta, F. Morier-Genoud, M. Moser, and U. Keller, "Q-switching stability limits of continuous-wave passive mode locking," J. Opt. Soc. Am. B **16**, 46-56 (1999).
26. J. Aus der Au, D. Kopf, F. Morier-Genoud, M. Moser, and U. Keller, "60-fs pulses from a diode-pumped Nd:glass laser," Opt. Lett. **22**, 307-309 (1997).
27. R. Paschotta, J. Aus der Au, G. J. Spühler, S. Erhard, A. Giesen, and U. Keller, "Passive mode locking of thin disk lasers: effects of spatial hole burning," Appl. Phys. B **72**, 267-278 (2001).
28. L. R. Brovelli, U. Keller, and T. H. Chiu, "Design and Operation of antiresonant Fabry-Perot saturable semiconductor absorbers for mode-locked solid-state lasers," J. Opt. Soc. Am. B **12**, 311-322 (1995).
29. M. Haiml, U. Siegner, F. Morier-Genoud, U. Keller, M. Luysberg, R. C. Lutz, P. Specht, and E. R. Weber, "Optical nonlinearity in low-temperature-grown GaAs: Microscopic limitations and optimization strategies," Appl. Phys. Lett. **74**, 3134-3136 (1999).
30. D. J. H. C. Maas, B. Rudin, A.-R. Bellancourt, D. Iwaniuk, T. Südmeyer, and U. Keller, "High Precision Optical Characterization of Semiconductor Saturable Absorber Mirrors (SESAMs)," presented at the Conference on Lasers and Electro-Optics (CLEO), San Jose, California, talk CThKK6, 2008.
31. S. V. Marchese, C. R. E. Baer, R. Peters, C. Kränkel, A. G. Engqvist, M. Golling, D. J. H. C. Maas, K. Petermann, T. Südmeyer, G. Huber, and U. Keller, "Efficient femtosecond high power Yb:Lu_2O_3 thin disk laser," Opt. Express **15**, 16966-16971 (2007).
32. E. R. Thoen, E. M. Koontz, M. Joschko, P. Langlois, T. R. Schibli, F. X. Kärtner, E. P. Ippen, and L. A. Kolodziejski, "Two-photon absorption in semiconductor saturable absorber mirrors," Appl. Phys. Lett. **74**, 3927-3929 (1999).
33. M. Haiml, R. Grange, and U. Keller, "Optical characterization of semiconductor saturable absorbers," Appl. Phys. B **79**, 331-339 (2004).
34. R. Grange, M. Haiml, R. Paschotta, G. J. Spuhler, L. Krainer, M. Golling, O. Ostinelli, and U. Keller, "New regime of inverse saturable absorption for self-stabilizing passively mode-locked lasers," App. Phys. B **80**, 151-158 (2005).
35. F. Brunner, R. Paschotta, J. Aus der Au, G. J. Spühler, F. Morier-Genoud, R. Hövel, M. Moser, S. Erhard, M. Karszewski, A. Giesen, and U. Keller, "Widely tunable pulse durations from a passively mode-locked thin-disk Yb:YAG laser," Opt. Lett. **26**, 379-381 (2001).

1 Introduction

Femtosecond sources with microjoule-level pulse energies are interesting for many scientific and industrial applications. The potential of short pulses to improve the processing quality of high-precision material ablation is well known [1], and the high peak intensities that can be obtained facilitate high field physics experiments. Both application areas benefit significantly from high pulse repetition rates in the megahertz regime to increase their throughput or improve the signal-to-noise ratio [2].

Until a few years ago, only complex and expensive laser systems were capable of generating ultrashort pulses with energy sufficient for these applications. The pulse energy of available diode-pumped femtosecond oscillators was limited to the few-nanojoule level, and

amplification by one or several amplifier stages was required. The limited average power of these systems resulted in repetition rates in the few-kilohertz regime. With the introduction of the thin disk laser [3], high average powers became possible in a power-scalable concept with excellent beam quality, the latter being a requirement for stable passive mode locking using semiconductor saturable absorber mirrors (SESAM) [4,5]. This combination resulted in femtosecond oscillators capable of directly generating microjoule-level pulse energies at multi-megahertz repetition rates with average powers of up to 80 W [6-8]. Pulse energies as high as 3 µJ have since been obtained with cavity-dumped systems operating at a repetition rate of 1 MHz [9,10]. Multi-megahertz femtosecond operation with few-microjoule pulses has been achieved with chirped-pulse fiber amplifiers based on a mode-locked seed oscillator and multiple amplifier stages [11]. To date, higher pulse energies of 50 µJ at megahertz repetition rates have only been obtained using complex fiber amplifier systems [12].

For lower noise performance and a more compact setup, it is beneficial to generate high-energy femtosecond pulses directly with a high-power mode-locked oscillator. This avoids the use of additional electronics and optical components for pulse picking and stretching, as well as compressing the pulses before and after the various amplifier stages. Oscillators typically show better pulse energy stability since spontaneous emission exerts a smaller influence than in amplifier systems. The pulse energy of high-power oscillators, however, has long been limited to the few-microjoule regime because nonlinearities of the air atmosphere inside the resonator destabilized the pulses. We have only recently been able to identify and eliminate the source of these instabilities and thereby increase the pulse energy to 5.1 µJ [13].

In this paper, we present the first femtosecond laser oscillator delivering pulse energies beyond the 10-µJ level without external amplification. It is based on a passively mode-locked Yb:YAG thin disk laser with a cavity extended to a total length of 37 m by means of a Herriott-type multiple-pass cavity (MPC) [14]. It delivers up to 45 W of average power at a repetition rate of 4 MHz when the laser resonator is flooded with gaseous helium to eliminate the Kerr-nonlinearity of the air atmosphere. The resulting 11.3-µJ pulses have a duration of 791 fs and a peak power of 12.5 MW and are delivered in a nearly diffraction-limited beam ($M^2 = 1.1$ measured at 9.4 µJ).

We will review the concept of the passively mode-locked thin disk laser, focusing on the key components required to obtain such high pulse energies directly from the laser oscillator. In section 2, we describe the thin disk laser head, the MPC used to extend the laser cavity and the SESAM design and parameters required to facilitate the high intracavity pulse energies. Section 3 contains the experimental results, and finally, the conclusions and an outlook are given in section 4.

2 Experimental setup

2.1 Yb:YAG thin disk laser head

The laser head used in this experiment is similar to the one described in [13]. The Yb:YAG gain medium has an Yb-doping concentration of ≈9 at.% and is cut and polished to a thickness of 200 µm. One end face of the disk is coated for high reflectivity at the pump and lasing wavelengths and directly soldered onto a water-cooled heat sink, while the opposite end face has an antireflective coating for the same spectral region. The disk is used in reflection and has a slight wedge (≈0.1°) to remove effects from residual reflections of the antireflective coating. With this geometry, one can obtain a high ratio of laser spot size to thickness of the gain medium, and thus the thermal gradients inside the gain material are nearly one-dimensional in the direction of the beam axis. Fundamental transverse mode operation has been achieved using such a geometry with up to 225 W of continuous-wave output power from a single disk [15]. For efficient absorption, the pump optics of our laser head are aligned for 24 passes through the disk with a pump spot diameter of 2.7 mm [16]. The pump light is delivered by a fiber-coupled diode laser emitting up to 230 W at 941 nm.

2.2 Importance of air inside the laser resonator

The generation of stable femtosecond pulses with a SESAM (see section 2.4) is realized using soliton mode locking, where the balanced effects of negative group delay dispersion (GDD) and self-phase modulation (SPM) lead to the formation of soliton-like pulses [17]. The negative intracavity GDD is introduced by a set of dispersive mirrors placed inside the resonator. In contrast to typical soliton mode-locked lasers, where the SPM arises mainly from small beam sizes and the resulting high intensity in the laser crystal, the gain medium in a thin disk laser contributes only a small amount of nonlinearity, due to its small thickness and the large mode size of the laser beam. A glass plate is therefore positioned in the laser beam at Brewster's angle to serve as a Kerr-medium for SPM and simultaneously ensure a linearly polarized output beam. The FWHM duration τ_p of the generated solitons for an intracavity pulse energy E_p is given by [17]

$$\tau_p \approx 1.76 \cdot \frac{2|D|}{|\gamma| E_p}.$$

(1)

For a laser cavity consisting of various discrete components, the roundtrip group delay dispersion D and SPM coefficient γ consist of the sum over all dispersive and nonlinear cavity elements. For a Gaussian beam, γ is given by

$$\gamma = \frac{2kn_2 L}{\pi w^2},$$

(2)

with $k = 2\pi/\lambda$ for the lasing wavelength λ in vacuum. The coefficient describes the nonlinear on-axis phase change $\Delta\varphi = \gamma P$ for a given optical power P, when propagating through a Kerr-medium with length L and nonlinear refractive index n_2. The beam radius w in (2) is assumed constant. This approximation is adequate for the SPM coefficients of the 1-mm-thick Brewster plate (γ_{BP}), as well as for the thin Yb:YAG disk (γ_{disk}). While good agreement with Eq. (1) was obtained with a thin disk laser operated at a repetition rate of 57 MHz [8], the experimental parameters obtained at a lower repetition rate of 34 MHz suggested the requirement of an additional unknown nonlinearity besides the one for disk and Brewster plate [6]. Since compensating for this additional nonlinearity would have required a substantial increase of the negative intracavity dispersion, the pulse energy remained limited to values below 2 μJ.

The unknown additional nonlinearity was later found to originate from the air atmosphere inside the laser resonator. The nonlinear refractive index of air is roughly three orders of magnitude lower than that of fused silica [18,19]. However, in a megahertz thin disk oscillator, the length of the path traveled in air is longer by a similar amount when compared to the thickness of the Brewster plate. The SPM coefficient of the air inside the laser cavity can thus be similar to or even considerably larger than γ_{BP}. We can estimate γ_{air} by integrating over the entire laser cavity:

$$\gamma_{air} = \frac{4kn_2}{\pi} \int_0^{L_{cav}} \frac{dz}{w^2(z)}$$

(3)

for a round-trip through the cavity with length L_{cav}. The contribution of the air to the total SPM coefficient obviously increases for longer cavities and hence lower repetition rates. Precise calculation of γ_{air} is made difficult by uncertainties about the nonlinear refractive index at 1030 nm for sub-ps-pulses. Moreover, precise knowledge of the beam parameters throughout the cavity are required. Nevertheless, estimations using the nonlinear refractive index $n_2 = 4 \cdot 10^{-19}$ cm²/W for 120-fs pulses at 800 nm from [18] show good agreement with the missing nonlinearity in [6], with $\gamma_{disk} \approx 0.1$ mrad/MW for the 100-μm-thin Yb:YAG disk, $\gamma_{BP} \approx 0.7$ mrad/MW for the Brewster plate, and $\gamma_{air} \approx 5$ mrad/MW for the path traveled in air. A relatively large amount of negative GDD (-22000 fs²) was used to compensate for this

significant additional nonlinearity from the air. Attempting to obtain stable mode locking at lower repetition rates by adding additional dispersive mirrors to increase the negative GDD becomes impractical, since the denominator in Eq. (1) scales approximately with L_{cav}^2 at constant average power.

For a further increase of the pulse energy, we therefore flooded the laser cavity with helium, which has a negligible nonlinearity compared with air, and successfully eliminated γ_{air}. This approach led to a significant increase of pulse energy to 5.1 μJ with the laser running at a repetition rate of 12.3 MHz [13]. Simple 4f extensions consisting of two mirrors spaced by their equal radius of curvature $R = 2f$ were used to lengthen the cavity to 12.2 m. This approach however becomes impractical when lowering the repetition rate to values well below 10 MHz, due to the amount of mirrors required.

2.3 Multiple-pass cavity and resonator setup

A convenient way to increase the resonator length is the use of a Herriott-type multiple-pass cavity (MPC) [14]. Similar to the 4f extensions used in [13], the q-parameter of a Gaussian beam is left unchanged when passing through an MPC, provided that the distance d between the curved mirrors is chosen appropriately. With a mechanism for injection and extraction of the beam, the MPC can therefore be added to an existing laser cavity, without affecting its mode size distribution or the point of operation in the stability zone [20]. Therefore the sensitivity towards thermal lensing remains unchanged.

This concept has already been successfully applied to low power Kerr-lens mode-locked Ti:Al$_2$O$_3$ oscillators [21], and more recently allowed increases in pulse energy towards the microjoule level with repetition rates of only a few MHz [22,23]. However, because these lasers are limited to a few watts of average power, pulse energies beyond the microjoule level have not yet been achieved with this approach. A comprehensive study of possible MPC configurations has recently been published in [24].

In its simplest form, an MPC consists of two mirrors of equal radius of curvature R, between which the beam passes multiple times to return to its starting point and complete a closed ray path (Fig. 1).
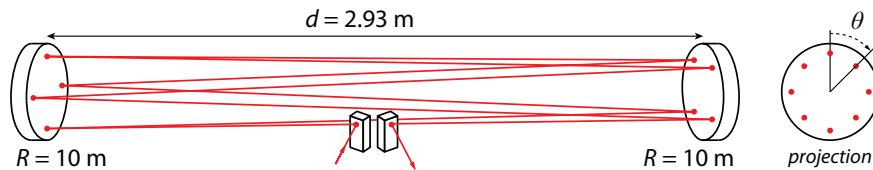

Fig. 1. Multiple-pass cavity (MPC) in a q-preserving configuration (left) with two curved mirrors ($R = 10$ m) spaced by $d = 2.93$ m for a total of $n = 8$ passes to form a closed ray path. Projection of the circular spot pattern on the two curved mirrors onto the x-y plane (right). The angle between two neighboring points on this projection is given by $\theta = 2\pi/n$.

For an even number of passes n from curved to curved mirror, the beam returns to its starting point and retraces its path if the distance is chosen according to [14]

$$d = R \cdot \left[1 - \cos\left(2\pi/n \right) \right]. \tag{4}$$

This re-entrant condition also leads to a q-preserving configuration. The MPC can then be aligned such that the $n/2$ beam spots on each of the curved mirrors form a circular pattern around the center axis of the system (Fig. 1, right). The angle between two spots on the projection of this pattern onto the x-y plane is given by $\theta = 2\pi/n$. For our MPC we chose $n = 8$ for a curvature of $R = 10$ m, which according to (4) leads to $d = 2.93$ m. The total distance propagated in the MPC is $D = n \cdot d = 23.4$ m. This configuration can be built more compactly when folded with an additional plane mirror as depicted in Fig. 2. For obvious reasons, this is typically described as a flat-curved configuration. However, with the definition of n being the

number of passes from curved to curved surface spaced by the distance *d*, the distinction of curved-curved and flat-curved configuration is unnecessary for an even number of passes, and Eq. (4) remains valid.
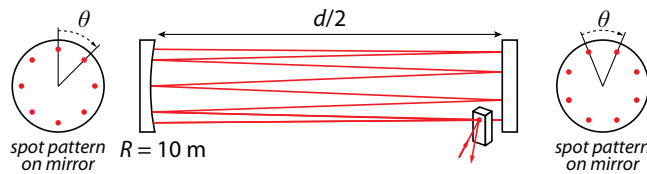

Fig. 2. Folded MPC with a single mirror for injection and extraction of the beam. The resulting spot patterns on the two MPC mirrors are shown to the left and to the right of the MPC. The angle between incident and extracted beam depends on the MPC geometry.

One important advantage of the configuration shown in Fig. 2 is that injection and extraction of the beam can be accomplished with a single additional mirror placed near the flat mirror of the MPC. This configuration has not been considered in the otherwise very comprehensive investigation of possible two-mirror MPCs given in [24], which predicts that the injection and extraction of the beam will always require two pickoff mirrors. However, the angle between the injected and extracted beam can not be freely adjusted when using a single pickoff mirror. As a result, the separation of the two beams is possible only after a certain propagation distance determined by the MPC geometry.

To further reduce the footprint of the MPC, an additional fold with a flat mirror can be achieved as shown in the schematic laser setup depicted in Fig. 3. The resulting laser cavity covers an area of approximately 50 cm by 150 cm and can easily be covered with the box required for helium flooding as described in section 2.2. The cavity further comprises a 4*f* extension to reach a final cavity length of 37 m. As depicted in Fig. 3, the MPC is inserted near the center of this 4*f* extension. The cavity length without the MPC is 13.7 m and the laser can thus be operated also at a repetition rate of 11 MHz. A total of 13 GTI-type dispersive folding mirrors (some not shown in Fig. 3) introduce a total negative dispersion of -20000 fs^2 per cavity round-trip. The Brewster plate has a thickness of 1 mm and is inserted near the output coupler, which has a transmission of 10% at 1030 nm. We estimate the total intracavity losses, not including output coupling, to be ≈6%. The reflectivity of the MPC mirrors is >99.98% according to the manufacturers specification.
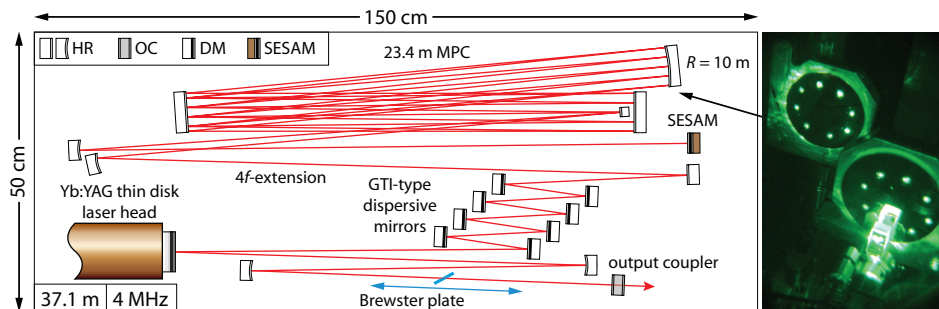

Fig. 3. Schematic of the laser setup with the 23.4-m-long MPC (not to scale). The total cavity length of 37 m results in a repetition rate of 4 MHz. The 1-mm-thick Brewster plate can be shifted along the direction of the divergent beam for fine-adjustment of the SPM and pulse duration. HR: highly reflective mirror, OC: output coupler (10%), DM: dispersive mirror, SESAM: semiconductor saturable absorber mirror.

The SPM coefficient of the 200-μm-thick disk in our laser is in the order of $\gamma_{disk} \approx 0.15$ mrad/MW, whereas γ_{BP} is about five times higher, depending on the beam size at

the actual position of the Brewster plate inside the cavity. Moving the Brewster plate along the axis of a divergent laser beam changes γ_{BP} and can thus be used to vary the pulse duration. The calculated SPM coefficient ($\gamma_{air} \approx 8.5$ mrad/MW) arising from the air in this 4-MHz cavity is similar to the one from the 12.3-MHz cavity ($\gamma_{air} \approx 8.4$ mrad/MW) used in [13] and not much larger than the one from the significantly shorter 34-MHz laser cavity ($\gamma_{air} \approx 5$ mrad/MW) used in [6]. This is because the beam radius remains relatively large ($w \geq 900$ μm) throughout the entire MPC and the $4f$ extension. The total value of γ_{air} is composed of the contribution from the MPC (≈ 4.5 mrad/MW), the $4f$ extension (≈ 2.2 mrad/MW) and the remaining part of the cavity (≈ 1.8 mrad/MW). The lengths of these three sections of the laser are 23.4 m, 10 m, and 3.6 m respectively.

2.4 Semiconductor saturable absorber mirror (SESAM)

We use a SESAM as an end mirror of the cavity for passive mode locking of the thin disk laser. The selection of appropriate absorber parameters is crucial to prevent mode locking instabilities such as Q-switched mode locking (QML) [25] or the formation of multiple pulses that simultaneously oscillate inside the resonator [6,26]. In the thin disk laser, QML can easily be prevented thanks to the high intracavity pulse energies and the additional stabilizing effects that arise from soliton formation [25]. The tendency for multiple pulsing is usually more critical, because the absorber is typically strongly saturated with pulse fluences more than ten times above the saturation fluence of the SESAM [6,13]. At such high saturation levels, the SESAM introduces only small loss penalties for closely spaced multiple pulses compared with a single soliton. Multiple pulses can thus profit from the gain advantage arising from their narrower bandwidth [27].

In order to prevent multiple pulsing, the SESAM saturation must be limited either by operating with large mode areas or increasing the saturation fluence of the device. For the current result we chose the latter approach, because the SESAM offers the unique possibility for wide tunability of the absorber parameters and therefore the cavity design must not be changed.

A straightforward method to increase the saturation fluence of a given SESAM is to reduce the field inside the absorber. For an antiresonant SESAM, this can be achieved by increasing the finesse of the device using a top mirror [28]. Because the modulation depth is reduced by this approach, one can introduce multiple absorber layers to facilitate sufficient modulation depth for stable passive mode locking.
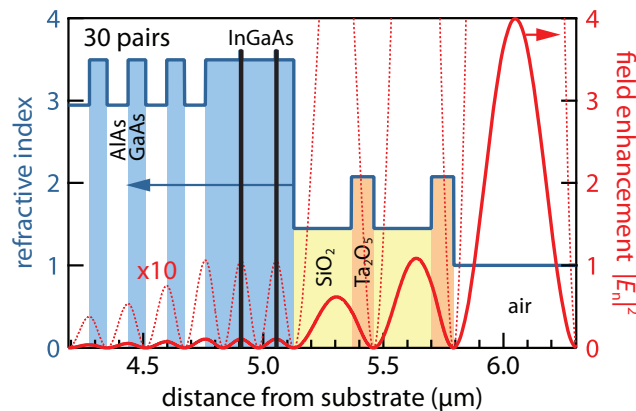

Fig. 4. Refractive index pattern and field enhancement of the antiresonant SESAM with a dielectric top mirror consisting of two pairs of alternating SiO_2/Ta_2O_5 layers. The SESAM has two 7-nm-thick InGaAs quantum well layers embedded in GaAs spacer layers to be positioned in the field maxima. The dotted red line is the field enhancement multiplied by a factor of 10.

Our SESAM is grown by molecular beam epitaxy (MBE) on top of a GaAs wafer. A distributed Bragg reflector (DBR) consisting of 30 pairs of alternating AlAs/GaAs quarter-wave layers serves as bottom mirror. Two 7-nm-thick InGaAs quantum well (QW) absorber layers embedded into GaAs spacer layers are grown on top of the DBR to be positioned in the maxima of the standing wave field pattern (Fig. 4). Low temperature growth of the absorber layers reduces the recovery time due to the arsenic antiside defects that act as very efficient traps for the electrons in the conduction band [29]. The top mirror consists of two pairs of alternating SiO_2/Ta_2O_5 layers deposited by electron beam evaporation. The thickness of these layers (240 nm SiO_2 and 93 nm Ta_2O_5) reduces the field enhancement in the absorber to ≈30% of its value in the uncoated device.

3 Experimental results

With the above-described experimental setup, we obtain stable passive mode locking at a repetition rate of 4 MHz with 45 W of average output power when the laser is operated in the box flooded with helium. The corresponding pulse energy is 11.3 μJ and the $sech^2$-shaped pulses have a duration of 791 fs (Fig. 5, left), resulting in a peak power of 12.5 MW. The pulses are nearly transform-limited ($\tau_P \Delta v = 0.35$, ideal: 0.315) with a spectral bandwidth of 1.56 nm centered at 1030 nm (Fig. 5, right). The beam quality is nearly diffraction-limited with an M^2-value of 1.1 (measured at 9.4 μJ). With ≈190 W of incident pump power, the optical-to-optical efficiency is 23.6%.
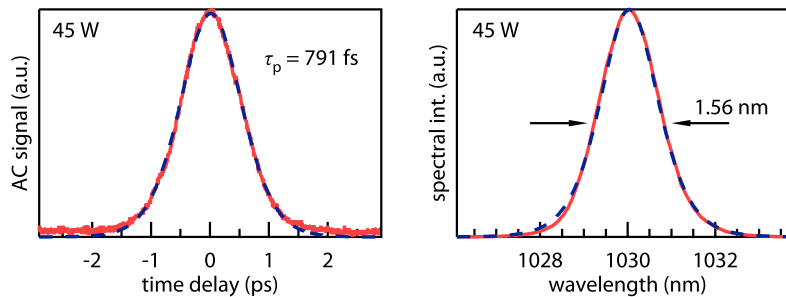

Fig. 5. Autocorrelation (left) and optical spectrum (right) of the 11.3-μJ pulses at 45 W of average output power and 4 MHz repetition rate. The blue dashed lines are fit-curves with an ideal $sech^2$-shaped pulse of 791 fs duration and an optical bandwidth of 1.56 nm. The soliton pulses are nearly transform-limited with a time-bandwidth product of 0.35 (ideal soliton: 0.315).

We traced the pulse train using a sampling oscilloscope with a fast photodiode (rise time: 18.5 ps) and a long-range autocorrelator with a scanning range of 80 ps. With the overlapping time windows of these measurements we can exclude the presence of multiple pulses inside the laser cavity. In addition, we measured the efficiency of second-harmonic generation (SHG) in a 5-mm-long critically phase-matched LiB_3O_5 (LBO) crystal. This measurement was performed in the regime of low conversion efficiency, with the output beam of the laser attenuated to a few watts. In this regime, the generation of the second-harmonic gives a good indication of single-pulse operation, because the conversion efficiency is significantly lower in the case of multiple pulsing owing to the reduced peak power. These measurements confirmed that we had a single pulse oscillating in the laser cavity.

The output power of the laser in this configuration is not limited by the available pump power, but by instabilities and multiple pulsing that occur when the laser power is further increased. Our calculations of the nonlinearity using Eq. (1) and (2) suggest that our helium box is not sufficiently airtight, such that a remaining air content of 5-10% prevents the complete elimination of γ_{air}. In combination with the strong SESAM saturation, this increases the tendency for multiple pulsing. Based on the calculated beam radius of ≈700-800 μm, we estimate the SESAM to be operated about 50-60 times above its saturation fluence, with a

corresponding pulse fluence of $\approx$5-7 mJ/cm^2. We used a high precision characterization setup to measure the reflectivity curve of the SESAM up to such high saturation levels [30]. This measurement was performed with a Yb:Lu$_2$O$_3$ thin disk laser operating at a laser wavelength of 1034 nm [31]. The pulse duration for the measurement was 570 fs. The resulting reflectivity curve is shown in Fig. 6 (left).
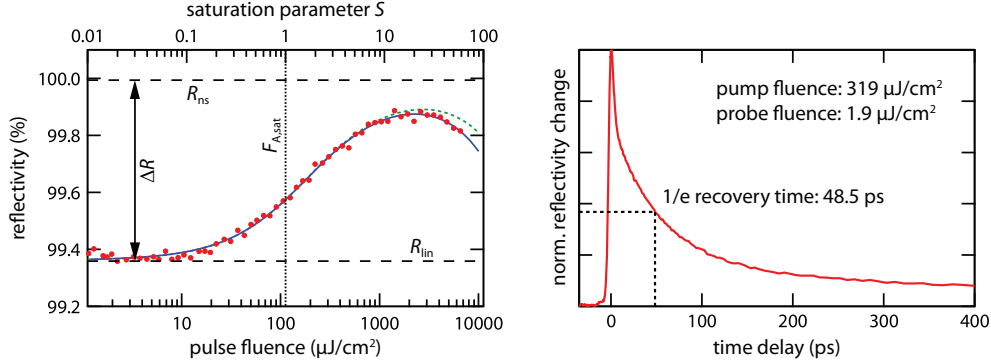

Fig. 6. Measured nonlinear reflectivity curve of the SESAM used for mode locking of the laser (left). The solid blue curve is the result of a fit using the model function (5), whereas the dotted green curve represents the SESAM reflectivity with a theoretically modified rollover for the longer pulses present in the Yb:YAG thin disk laser. SESAM recovery measured with a pump probe setup using 2.5-ps pulses at 1030 nm (right).

In addition to the typical saturation behavior, a rollover at high pulse fluences is observed, which causes the reflectivity to decrease after reaching a maximum value. This effect has already been observed at much lower pulse fluences in the order of 100 μJ/cm^2 or below in SESAMs with higher field enhancement factors, i.e., larger field intensities inside the semiconductor structure [32,33]. For femtosecond pulses, this rollover is attributed to two-photon absorption (TPA) in the GaAs semiconductor material and has been exploited to reduce the tendency for QML in high repetition rate lasers with low pulse energies [34]. TPA causes higher losses for higher pulse fluences and effectively counteracts the saturation of the absorber. The corresponding change of the reflectivity curve $R(F_P)$ can be modeled by an additional rollover coefficient F_2

$$R\left(F_P\right) = R_{ns} \cdot \frac{\ln\left(1 + R_{lin}/R_{ns} \cdot (e^{F_P/F_{A,sat}} - 1)\right)}{F_P/F_{A,sat}} \cdot e^{-F_P/F_2} \, , \tag{5}$$

where $F_P = E_P/(\pi w^2)$ is the pulse fluence, R_{ns} is the reflectivity at infinite pulse fluence in absence of the rollover, R_{lin} is the linear reflectivity of the unsaturated SESAM, $F_{A,sat}$ is the saturation fluence, and $S = F_P/F_{A,sat}$ used in Fig. 6 is the saturation parameter. The coefficient F_2 for $sech^2$-shaped pulses is given by an integral over the entire SESAM structure [34]

$$F_2 = \frac{\tau_P}{0.585 \cdot \int \beta(z) n^2(z) \left(\left|E_n(z)\right|^2\right)^2 dz} \, , \tag{6}$$

with local TPA coefficient $\beta(z)$ and refractive index $n(z)$. $\left|E_n(z)\right|^2$ is referred to as the field enhancement with $E_n(z)$ being the local electric field, normalized to 1 for the incident wave. The derivation of Eq. (5) and (6) are given in [33,34], along with some modifications required to model Gaussian beams.

The absorber parameters were determined using the model function (5). The SESAM has a saturation fluence of $\approx$115 μJ/cm^2, a modulation depth of $\approx$0.6%, and low non-saturable

losses of less than 0.1% (Fig. 6, left). The rollover coefficient F_2 was measured to be 4.4 J/cm^2 for the 570-fs pulses from the Yb:Lu$_2$O$_3$ laser. Because F_2 is directly proportional to the pulse duration, we can use Eq. (6) to calculate the value for the 800-fs pulses in the Yb:YAG thin disk laser to be $F_2 \approx 6.1$ J/cm^2. The corresponding reflectivity curve is depicted by the green dotted line in Fig. 6. According to this estimate, with the maximum pulse energy of 11.3 µJ we begin to enter a regime where the reflectivity of the SESAM decreases with increasing pulse energy. We can therefore conclude that the limitation of the pulse energy encountered in our laser is most likely caused by the rollover of the currently used SESAM: Once the reflectivity on the SESAM has reached its maximum, a further increase in pulse energy would result in a loss penalty for the single soliton, such that multiple pulsing would become more favorable. We further used a pump-probe setup with 2.5-ps pulses at 1030 nm to measure the recovery time of the SESAM. Fig. 6 (right) shows the temporal response at a pump fluence of 319 µJ/cm^2 with a 1/e recovery time of 48.5 ps.

One can reduce the strength of TPA and thus further increase the pulse energies if the duration of the pulses is increased, e.g., by adding more negative GDD to the laser cavity. In most cases, however, this is undesirable because many applications profit from shorter pulse durations. To reduce the rollover while keeping the pulse duration constant, one can, for example, replace the GaAs spacer layers by AlAs as demonstrated in [34], because AlAs has a negligible TPA coefficient. In this paper, we instead use a top mirror consisting of dielectric materials that do not exhibit any TPA. We can thus simultaneously increase the saturation fluence of the device and minimize the strength of the rollover. In comparison, a SESAM from the same growth but without any top mirror shows a much stronger rollover with $F_2 \approx 1.2$ J/cm^2, because the field enhancement inside the semiconductor material is much higher.

4 Conclusion and outlook

In conclusion, we have demonstrated the first femtosecond laser oscillator producing pulse energies beyond the 10-µJ level without external amplification. We obtain 45 W of average power at a repetition rate of 4 MHz from a passively mode-locked Yb:YAG thin disk laser. The 11.3-µJ output pulses have a duration of 791 fs and the resulting peak power is 12.5 MW. The significant increase in pulse energy was made possible by extending the cavity length to 37 m using a Herriott-type MPC and by operating the laser in a helium atmosphere in order to eliminate the air nonlinearity.

The current result is limited by strong saturation of the SESAM, which shows a rollover of the reflectivity when operated with the relatively high pulse fluences. As a consequence, further increase of the pulse energy currently results in instabilities and multiple pulsing. Moreover, the limited airtightness of the helium box appears to prevent the complete elimination of the air nonlinearity. Both limitations can easily be overcome by improvements of the experimental setup. To prevent the large SESAM saturation, the mode area on the SESAM or the saturation fluence can be increased using a more sophisticated SESAM design: Increasing the number of quantum wells simultaneously with the number of layers in the dielectric top mirror will result in SESAMs that exhibit yet higher saturation fluences while the field inside the semiconductor layers is further reduced, which ultimately reduces the rollover caused by TPA. With these changes we expect this concept to allow even higher pulse energies in the future. The experimental setup can further be simplified using MPC-mirrors with a dispersive coating, such that the additional GTI-type dispersive mirrors are no longer required.

Reducing the intracavity pulse energy would be an additional possibility for reducing the strong saturation of the SESAM as well as the SPM caused by the nonlinearity of the air: A simultaneous increase of the output coupling and the number of passes through the gain medium can be used to reduce the intracavity pulse energy while keeping the output power constant. Multiple passes over the disk, however, may result in the generation of longer pulses because the spatial hole burning in the disk can be largely wiped out [27,35]. More efficient performance is further expected using Yb:Lu$_2$O$_3$ as gain medium [31]. The broader

amplification bandwidth of this material allows the generation of shorter pulses with the additional benefit that higher intracavity nonlinearities can be tolerated. Finally, we expect that the output pulse energy can be further increased by combining multiple laser heads inside one resonator. If the output coupler transmission is increased accordingly, the intracavity pulse energy and thus the nonlinearities remain unchanged.